Surface & Coatings Technology 275 (2015) 357–362

Contents lists available at ScienceDirect

Surface & Coatings Technology

journal homepage: www.elsevier.com/locate/surfcoat

Electrochemical vs antibacterial characterization of ZrCN–Ag coatings

S. Calderon V [a,d,*], I. Ferreri [a,b], R. Escobar Galindo [c], M. Henriques [b], A. Cavaleiro [d], S. Carvalho [a,d]

[a] GRF-CFUM, Physics Department, University of Minho, 4800-058 Guimarães, Portugal
[b] IBB, University of Minho, Campus of Gualtar, 4700-057, Portugal
[c] Instituto de Ciencia de Materiales de Madrid (ICMM-CSIC), Cantoblanco, 28049 Madrid, Spain
[d] SEG-CEMUC Mechanical Engineering Department, University of Coimbra, 3030-788 Coimbra, Portugal

ARTICLE INFO

Article history:
Received 25 November 2014
Accepted in revised form 24 April 2015
Available online 30 April 2015

Keywords:
Silver
Antibacterial
ZrCN
EIS
GD-OES
Electrochemical behavior

ABSTRACT

Nowadays, antibacterial properties are becoming a viable feature to be introduced in biomaterials due to the possibility of modifying the materials' surface used in medical devices in a micro/nano metric scale. As a result, it is mandatory to understand the mechanisms of the antimicrobial agents currently used and their possible failures. In this work, the antibacterial activity of ZrCN–Ag films is studied, taking into consideration the ability of silver nanoparticles to be dissolved when embedded into a ceramic matrix. The study focuses on the silver release evaluated by glow discharge optical emission spectroscopy and the effect of the fluid composition on this release. The results revealed a very low silver release of the films, leading to non-antibacterial activity of such materials. The silver release was found to be dependent on the electrolyte composition. NaCl (8.9 g L^{-1}) showed the lowest spontaneously silver ionization, while introducing the sulfates in Hanks' balanced salt solution (HBSS) such ionization is increased; finally, the proteins incorporated to the (HBSS) showed a reduction of the silver release, which also explains the low ionization in the culture medium (tryptic soy broth) that contains high quantities of proteins.

1. Introduction

Antibacterial materials have been extensively studied during the last decades with the aim of using them in biomedical devices. One effective approach has been the modification of existing materials to provide them with functional properties that allow their use as biomaterials [1,2]. An efficient mean of producing those changes is to provide the materials' surface with additional layers to enhance their mechanical, chemical characteristics and antimicrobial capabilities, reducing implants failure. Clear examples of these modifications are protective films deposited by physical or chemical vapor deposition [3–11]. Our group has demonstrated the protective effect of ZrCN coatings doped with silver nanoparticles, maintaining or even improving the corrosion resistance of 316L stainless steel [12].

Silver, on the other hand, has been reported to be an excellent antimicrobial agent with a very large spectrum against bacteria and fungus [9,13–17]. The mechanism to explain the mode of operation of such element is not well established, and thus, both silver ions and silver nanoparticles have been considered as proper antibacterial agents [18,19]; furthermore, neutralizing agents, such as amino acids containing thiol groups present in the human body have been also identified to reduce the silver antimicrobial capacity [19–22]. As a result, the antibacterial activity of the system does not only depend on the composition of the material but also on the medium in which it is studied.

Several reports have described the antibacterial activity promoted by silver in ceramic matrices such as nitrides, emphasizing that the higher the silver content in the films the higher the antibacterial behavior is attained. Hsieh et al. [8], for instance, have studied the antibacterial effect of TaN–Ag with 1.6 to 10 at.% of silver on *Escherichia coli*, and found that the latter has the higher effect. They associated the antimicrobial results to a hypothetical rise on the silver ion concentration in the solution. Kelly et al. [9] studied the Zr, Ti and Cr nitrides with different silver contents and verified that the antibacterial effect on *Pseudomonas aeruginosa*, or *Staphylococcus aureus* was more evident by increasing the silver content, but they also showed that the effect was dependent on the methodology used to evaluate the antibacterial performance. Baghriche et al. [10], on the other hand, demonstrated that Ag–ZrN films deposited by magnetron sputtering improved the antibacterial effect compared to Ag–N surfaces using large amount of silver (13 to 63 at.%). Nevertheless, these reports do not clearly specify the culture medium used, hampering the analysis about the influence of the media in the antibacterial activity.

Our group has previously reported the lack of antibacterial effect in Ag–TiCN coatings deposited with different silver content [23], which promoted bacteria adhesion due to the increase of high density apolar areas on the surface. In addition, other reports such as Kelly et al. [9] have shown the absence of these effects in similar materials. Nonetheless, the lack of the antibacterial effect of silver in such matrices

* Corresponding author at: Universidade do Minho, Dept. Física, Campus de Azurém, 4800-058 Guimarães, Portugal. Tel.: +351 253510175x517469; fax: +351 253510461.
E-mail address: secave44@gmail.com (S. Calderon V).

http://dx.doi.org/10.1016/j.surfcoat.2015.04.042
0257-8972/

is not very well understood. Therefore, the main aim of this work, was to evaluate the evolution of the silver release from ZrCN–Ag films immersed in four electrolytes having different compositions, in order to better understand the interaction of the film components and the electrolyte composition and their role in the antibacterial activity.

2. Material and methods

2.1. Coating production

Zirconium carbonitride coatings with silver nanoparticles (ZrCN–Ag NPs) were deposited by dual reactive magnetron sputtering onto 4 cm^2 316L stainless steel (SS316L) and Si (100) substrates, as described elsewhere [24]. Briefly, the samples were cleaned in an ultrasonic bath using distilled water, ethanol and acetone for 10 min in each fluid. The substrates were etched with argon ions for 1200 s and the films were deposited using 60 sccm of Ar flux, 4 sccm of nitrogen and 1.2 sccm of acetylene flux, maintaining the target density current at 2.5 mA cm^{-2} for the Zr–Ag target and 7.5 mA cm^{-2} for the Zr target. The distance between the substrates and the target (70 mm), as well as the temperature (373 K) and the bias voltage (−50 V) remained constant during the depositions. The combination of these parameters provides a deposition rate of 1.7 μm h^{-1}. The density current in the targets was selected in order to attain a specific percentage of silver in the film (11 at.%), taking into consideration that this is the silver content used to attain antibacterial effect in the current state of the art for similar materials.

2.2. Chemical depth profile composition

Glow discharge optical emission spectroscopy (GD-OES) was utilized to evaluate the compositional profile of the as-deposited samples and after immersion. The tests were performed using a Jobin Yvon RF GD Profiler equipped with a 4 mm diameter anode and operating at a typical radio frequency discharge pressure of 650 Pa and a power of 40 W. The emission lines detected were oxygen (130.217 nm), nitrogen (149.262 nm), carbon (156.14 nm), silver (328.08 nm), nickel (341.447 nm), phosphorous (178 nm), chromium (425.433), sulfur (181 nm), zirconium (339 nm) and iron (271.441 nm). The calibration of the light elements such as N was carried out as explained in [25]. The calibration of oxygen and carbon was carried out by standard materials. However, special care must be taken with the carbon quantification due to the lack of standards with large amount of carbon and large sputtering rates similar to the ones presented in this work.

2.3. Biological assays

Bacterial colonization assays were performed using the IE186 strain of *Staphylococcus epidermidis*. This strain was stored at −80 °C in glycerol stocks until use. Cells were firstly grown for approximately 36 h in tryptic soy agar (TSA, Merck) plates, and then incubated for 18 h in tryptic soy broth (TSB, Merck), at 37 °C under a constant agitation of 120 rpm. After that, cells were centrifuged for 5 min at 8900 *g* and 4 °C and carefully washed with a phosphate buffer saline (PBS), alternating this process twice. The cellular suspension (TSB and cells) was adjusted to the final concentration of approximately 1×10^8 cells mL^{-1}, determined by optical density at 640 nm (using the software ELISA).

The samples with 4 cm^2 in area (previously sterilized at 121 °C for 15 min) were placed in six-well plates with 3 mL of the cellular suspension in each well. The plates were incubated at 37 °C under a constant agitation of 120 rpm for 2 h (adhesion) and 24 h (biofilm formation).

After incubation of *S. epidermidis*, all the supernatant was removed and the coatings were gently washed with PBS to remove non-attached bacteria. The remaining adherent bacteria were detached from the coatings using an ultrasonic bath for 10 min in 3 ml of fresh PBS medium. The bacteria were incubated with serial dilutions on TSB agar plates at 37 °C for 24 h, and the number of CFUs (colonies forming units) was counted. Experiments were run in triplicate per sample (technical replicates) and on three independent occasions (biological replicates).

Scanning electron microscopy was used to observe bacterial adhesion and biofilm formation on the surface of the coatings. After adhesion and biofilm formation the coatings were carefully washed three times with distilled water. Samples were dehydrated by immersion in increasing ethanol concentration solutions: 70, 95 and 100% (v/v) for 10, 10 and 20 min, respectively, and placed in a sealed desiccator. Afterwards, the samples were mounted on aluminum bases with carbon tape, sputter-coated with gold and observed with a Leica S360 scanning electron microscope. In order to assess the extent of bacterial adhesion and biofilm formation in each sample, three fields were used for image analysis.

2.4. Electrochemical characterization

The films were evaluated electrochemically by electrochemical impedance spectroscopy (EIS) and potentiodynamic anodic polarization. The tests were performed by means of a Gamry REF600 potentiostat on the coated SS316L substrates using a classic water-jacketed 200 ml corrosion cell, using a platinum plate as counter electrode and saturated calomel (SCE) as reference electrode. Samples with 1.73 cm^2 of exposed area were immersed into four different simulated body fluids in order to evaluate the influence of their components on the electrochemical activity of the ZrCN–Ag coatings. Sodium chloride solution concentrated at 8.9 g L^{-1} (NaCl) was prepared as the simplest electrolyte solution, to evaluate the influence of chloride ions on the silver release. Then, phosphates and sulfates were also studied by a Hanks' balanced salt solution (HBSS). In addition, 10 g L^{-1} of albumin was added to the HBSS (HBSS + A) in order to equate the synovial fluid conditions and evaluate its reactivity with the materials. Finally, tryptic soy broth (TSB) solution used for bacterial growth was analyzed in order to assess the effect of this solution on the silver activity. The later fluid was also studied to determine the different electrochemical behavior when the material is subjected to biological tests, clarifying if the medium can significantly affect the biological assays. All the electrolytes were set at 37 °C to better simulate the body conditions and the samples were immersed for 7 days.

The electrochemical impedance spectra were collected as a function of time at 2 h, 48 h and 168 h and correlated with the surface characterization performed by glow discharge optical emission spectroscopy (GD-OES). Before each impedance spectrum, a stable open circuit potential (OCP) was achieved in order to guarantee the sample stability in the electrolyte and a sinusoidal ac perturbation of 10 mV vs SCE amplitude was applied to the electrode over the frequency range 0.1 Hz–100 kHz.

Potentiodynamic tests were performed on samples after one hour of immersion to achieve a stable OCP potential, using a scanning rate of 60 mV/min from −500 mV vs. OCP to +1800 mV vs. OCP.

The results of the electrochemical test were calculated as the average and standard deviations of at least three separate samples. All the potentials are expressed with respect to SCE electrode.

3. Results and discussion

The films were previously chemically and structurally characterized, and the results can be found in a previous publication [24]. Briefly, the material is composed of a $ZrC_{0.35}N_{0.65}$ crystalline phase, as well as an amorphous carbon phase, and metallic silver nanoparticles. Zirconium oxides are also observed on the surface of the films, while silver was identified only in metallic state and well distributed in the film. The thickness of the films is around 700 nm with roughness (Ra) lower than 50 nm and a bulk composition of 32.2 at.% of Zr, 28.3 at.% of N,

19.1 at.% of C, 11.1 at.% of Ag and residual O around 9.3 at.%, obtained by electron probe microanalysis. The element distribution through the film depth is shown in Fig. 1a, while the first 50 nm is shown in Fig. 1b, revealing the formation of a top film rich in silver with a few nanometers of thickness. This silver agglomeration on the surface has been previously reported for similar systems and explained by the reduction of the surface energy of the particles by increasing their sizes [26,27].

In order to determine the antibacterial effect of the films, the cellular viability, determined by colony forming units (CFUs), was measured after 2 and 24 h of exposure to the cellular suspension and is represented in Fig. 2. ZrCN films without silver were used as control sample for the experiments. Unexpectedly, the results showed that ZrCN with silver nanoparticles (ZrCN–Ag) do not present any antibacterial activity; on the contrary, these samples seem to promote a statistically significant increase ($p < 0.05$) of the biofilm biomass after 24 h (Fig. 2). These results were confirmed by scanning electron microscopy, in which bacterial adhesion was observed after 2 h in contact with the bacteria suspension, increasing in quantity as the exposure time increases, revealing a biofilm after 24 h (Fig. 3). Similar results were reported by Carvalho et al. [23], for TiCN–Ag, giving a possible explanation of such increase due to the higher hydrophobic character of the films when silver is incorporated, which promoted the bacteria adhesion, increasing the affinity between the bacteria cells and the surface. The high hydrophobicity character is also corroborated in the ZrCN–Ag, showing contact angles of 106 ± 3° in distilled water. However, the reason for the absence of silver antibacterial activity in these types of matrices remains unclear. In similar matrices, Wickens et al. [28] have demonstrated that the increase of silver in the coatings (between 15 to 30 at.%), the respiring colonies on the surface significantly decreased in ZrN–Ag coatings compared to pure ZrN coatings, for *S. aureus* and *S. epidermidis*. Furthermore, antibacterial properties of ZrN–Ag were reported against *S. epidermis*, *S. aureus*, and *E. coli*. However, different initial cell concentration and antibacterial methodologies were used in these studies, hindering the direct comparison of the results and the explanation of the contradictory results [29].

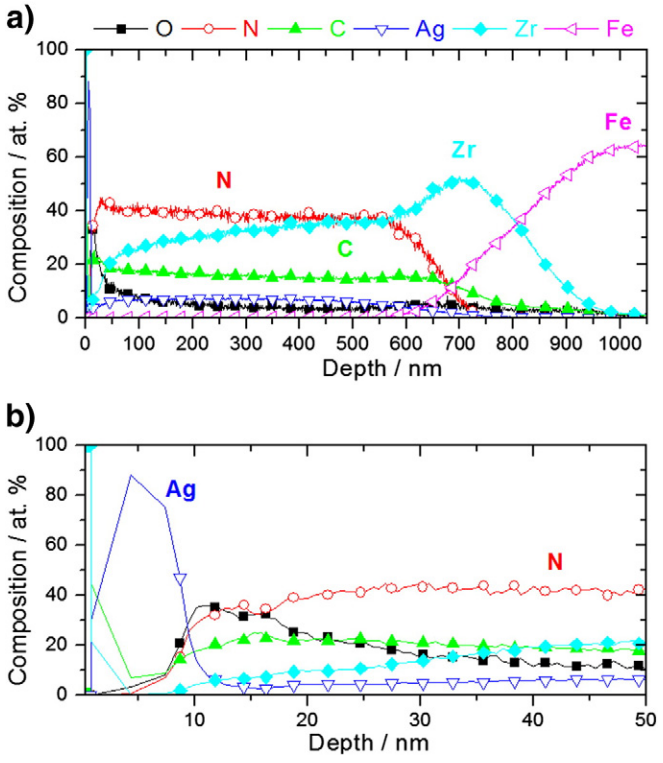

Fig. 1. a) Compositional depth profile of ZrCN–Ag for as-deposited samples and b) ZrCN–Ag compositional depth profile enlargement for the first 50 nm. The lines represent the experimental results, while the symbols are used to differentiate the elements.

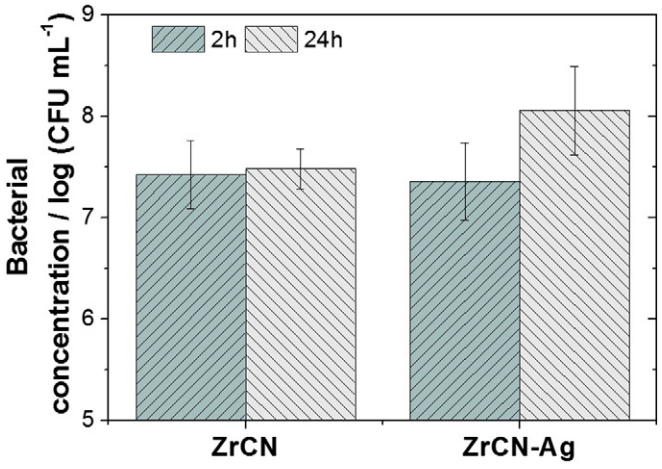

Fig. 2. Logarithm of bacterial concentration after 2 and 24 h contact between ZrCN–Ag, ZrCN coatings and *S. epidermidis*.

There is still a controversy in the literature about how silver kills bacteria. Two main mechanisms have been differentiated. Firstly, silver nanoparticles, which are sufficiently small (<12 nm) to penetrate the bacterial cellular wall, cause structural changes in the cell membrane, creating small holes and promoting the death of the cells [18]. Secondly, silver ions can interact with the cell thiol groups, binding to the main functional groups in some components such as enzymes, and avoid bacterial division, damaging the cell envelope [19]. In both cases, active antibacterial effect is exhibited when silver is released from the material, and thus, it is mandatory to understand which of these cases is more likely to occur in ceramic matrices and the reason why such release is not taking place in our coatings in order to be able to activate and control such mechanisms.

Considering that silver nanoparticle detachment from the surface is less probable, the mechanism for silver antibacterial behavior in ceramic matrices should be due to silver ionization, highly dependent on the electrochemical reaction occurring between the surface material and the electrolyte. As a result, the samples were electrochemically evaluated in four different types of electrolytes, in order to evidence the effect of the electrolyte composition in the silver release. The assays were complemented by a surface composition analysis and a morphological analysis of the samples before and after immersion.

Fig. 4 shows the open circuit potential (OCP) measured for the four electrolytes as a function of the immersion time. Different tendencies are evidenced depending on the electrolyte composition. NaCl at 0.89% w/v (NaCl) and Hanks' balanced salt solution (HBSS) exhibit an increasing trend with increasing immersion time, typical of materials with passive behaviors in which compounds with low electrochemical activity are formed. However, Hanks' balanced salt solution with 10 g L^{-1} of albumin (HBSS + A) and tryptic soy broth (TSB) electrolytes showed an opposite behavior, a decrease in the OCP was observed as the immersion time in the electrolyte increased. A similar behavior has been reported for metallic samples in albumin-containing electrolytes; protein addition to the electrolyte induced an immediate drop of OCP value due to the albumin adsorption [30]. Thus, the decrease of the OCP values for HBSS + A and TSB may be explained by protein adsorption on the coatings' surface, such as the albumin and the casein present in the electrolytes, respectively.

Fig. 5 shows the potentiodynamic curves for all the electrolytes. All the material-electrolyte combinations showed similar current densities and corrosion potentials, indicating similar electrochemical behavior for all electrolytes. However, the passivation currents were higher for NaCl, decreasing for HBSS and further reduced for the protein-containing electrolytes, which may indicate that components such as phosphates, sulfates and proteins help to passivate the surface of the material (Fig. 5 inset). The samples immersed into TSB showed the higher

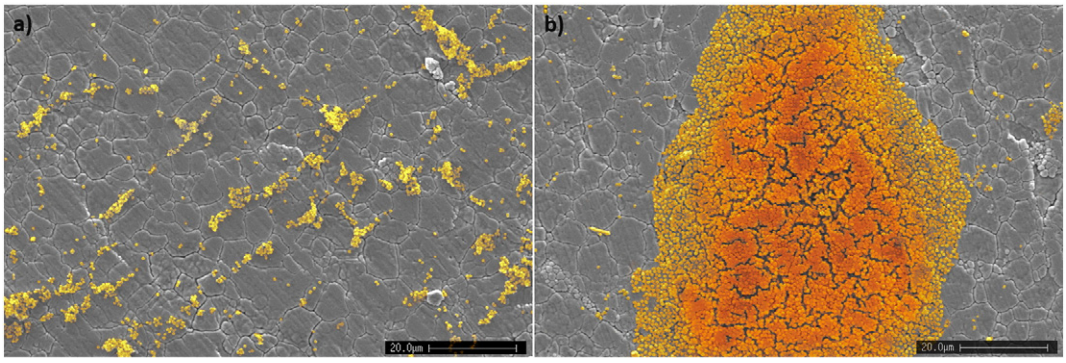

Fig. 3. False color scanning electron microscope images of ZrCN–Ag after a) 2 h b) 24 h in contact with *S. epidermidis*. The colored parts of the images corresponds both individual bacteria and bacterial colonies.

range of potentials in the passivation zone, indicating that this fluid prompt a more stable passive film on the ZrCN–Ag surface. This is explained due to the existence of a higher protein concentration in TSB (17 g L^{-1} of casein peptone and 3 g L^{-1} of soy peptone) compared to HBSS + A (almost twice). The proteins on the surface impede the access of the oxidant agents of the electrolytes with the material surface, and therefore, as one of the half-reaction in the oxidation-reduction process decreased, the rate of the counterpart reaction is also reduced. This complete process may also decrease the silver ionization on the fluids containing proteins and reduce the antibacterial effect of the silver. The loss in the antibacterial activity of silver in the presence of proteins has previously been reported and attributed to the amino acid containing thiol groups. They can bond to silver ions avoiding their contact with the bacteria, neutralizing the antibacterial effect [19–22].

Fig. 6 displays the Nyquist plots of the ZrCN–Ag samples immersed into the four electrolytes as a function of the immersion time. All samples presented similar tendencies as a function of time, increasing the immersion time, the samples' impedance increased. This behavior represents an improvement in the corrosion resistance of the materials due to the formation of stable compounds that blocks the electrolyte penetration into the coatings. This blocking behavior is enhanced by adding components such as phosphates, sulfates and proteins for the case of HBSS, HBSS + A and TBS. The impedance tends to increase, revealing the protective behavior induced by the formation of protective layers that block the paths for the electrolyte, in agreement with their lower passive current determined by potentiodynamic tests.

The formation of such protective compounds is confirmed by GD-OES results. Fig. 7 shows the formation of very thin films rich in oxygen on the films' surface in all the electrolytes; in the case of HBSS and TSB fluids phosphorus and sulfur are observed, indicating the formation of additional compounds with those elements. The incorporation of the electrolytes into the films takes place in only around the first 15 nm of the material, and therefore, the contact between the electrolyte and the interface film-substrate is discarded for the immersion time studied. Zr–C–N elements were also analyzed after immersing the samples in the electrolytes (Fig. 8), showing a very stable surface. It must be stressed that samples were cleaned with water and ethanol in an ultrasonic bath for 10 min after being in contact with the electrolyte, which reveals that the compounds observed in the GD-OES are linked to the surface forming stable compounds with the films' surface.

Silver evolution, on the other hand, is individually presented in Fig. 9 exhibiting a reduction in all the electrolytes but in different proportions. It must be stressed that more than three as-deposited samples were analyzed in order to guarantee that the changes on the silver distribution were due to the electrolyte interaction and not due to the production process (inset of Fig. 9). The changes in the silver content on the first 15 nm were attributed to the silver ion release to the media. This release was found to occur in the early hours of the immersion tests and further release was not observed in all media (cf. Fig. 9 inset), which indicates that the protective layer formed by oxides, sulfides and/or protein adsorbed on the surface may prevent the silver to be released to the electrolyte.

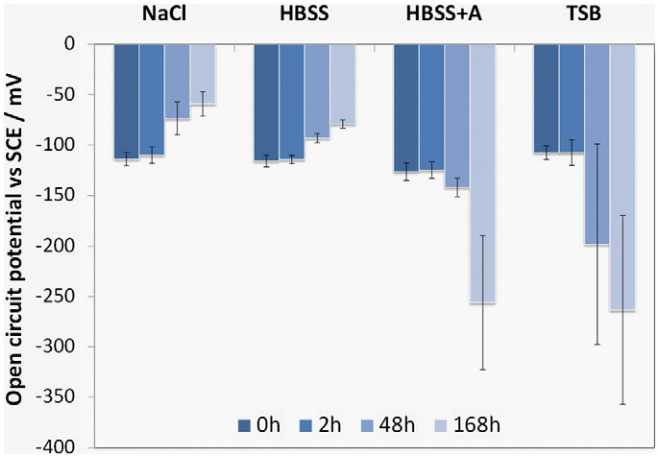

Fig. 4. Open circuit potential evolution of ZrCN–Ag coatings for 168 h in four different electrolytes, NaCl, Hanks' balanced salt solution (HBSS), HBSS with 10 g of albumin per liter (HBSS + A), and tryptic soy broth (TBS).

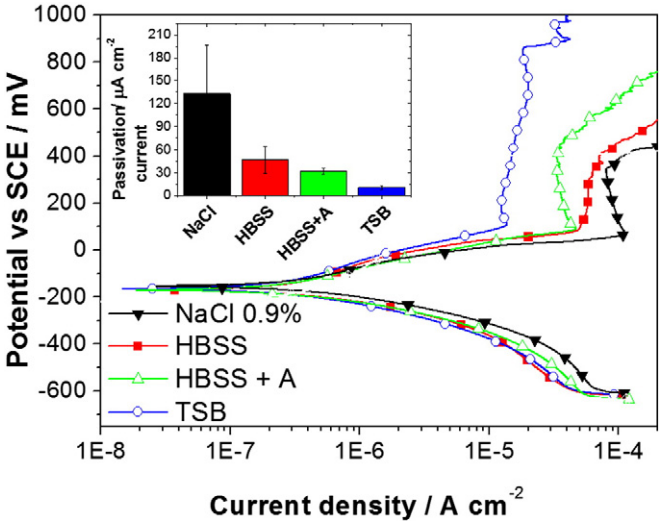

Fig. 5. Potentiodynamic curves of ZrCN–Ag coatings in four different electrolytes, NaCl, Hanks' balanced salt solution (HBSS), HBSS with 10 g of albumin per liter (HBSS + A), and tryptic soy broth (TBS). Inset: Passivation current of ZrCN–Ag coatings in the four electrolytes.

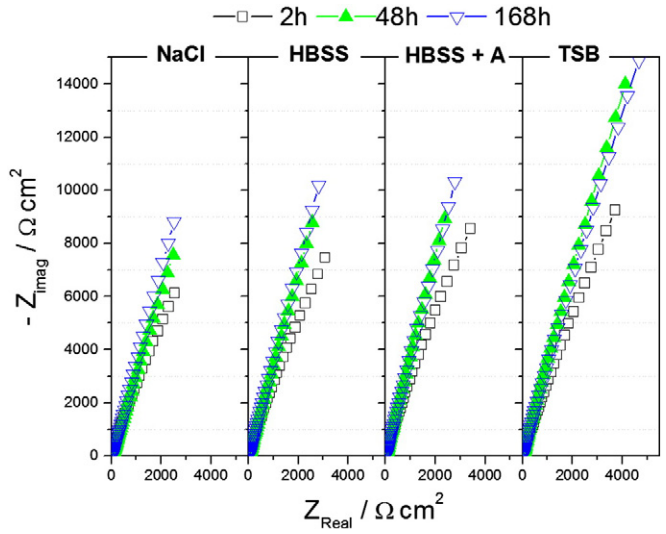

Fig. 6. Nyquist plot evolution of ZrCN–Ag coatings as a function of immersion time in four different electrolytes, NaCl, Hanks' balanced salt solution (HBSS), HBSS with 10 g of albumin per liter (HBSS + A), and tryptic soy broth (TBS).

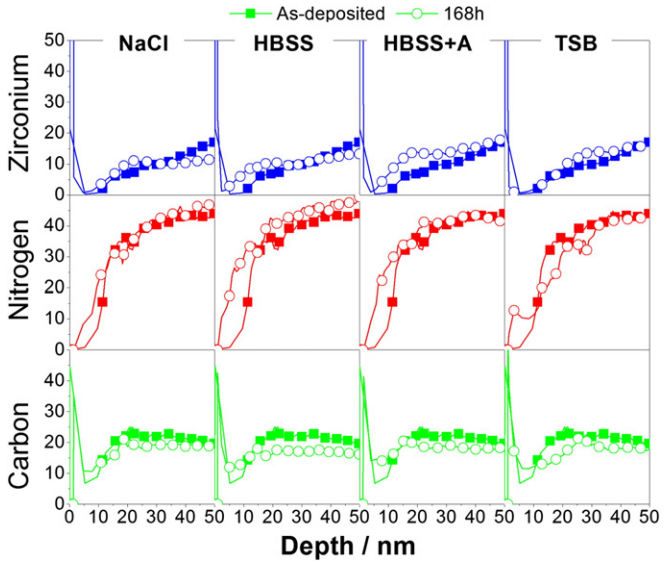

Fig. 8. Zirconium, nitrogen and carbon depth profile of ZrCN–Ag for as-deposited (▪) samples and after 168 h (o) of immersion in NaCl, Hanks' balanced salt solution (HBSS), HBSS with 10 g of albumin per liter (HBSS + A), and tryptic soy broth (TBS). The lines represent the experimental results, while the symbols are used to differentiate the elements.

The different behavior of silver on each electrolyte demonstrates the relevance of the fluid components in the electrochemical activation of silver. The simplest electrolyte (NaCl) limits the production of silver ions, since it is expected that Cl^- ions react with the silver in the films, forming insoluble products such as AgCl, that protect the material. However, as shown in Fig. 9, by introducing the sulfates in the electrolyte composition (HBSS) a higher silver released was observed, in agreement to Beyer [31] who reported that $MgSO_4$ accelerated the dissolution of silver nanoparticles. HBSS and HBSS + A additionally show the influence of protein in the silver ion release, since the reduction of the silver on the surface is lower when albumin is present in the fluid. In TSB, on the other hand, despite being a complex electrolyte the presence of the sulfur came only from the amino acids with thiol groups existing in the proteins, and therefore, the silver ionization may decrease due to the adsorption of such compounds on the surface, as well as the increasing phosphates on the surface. Despite the different behavior on the silver release, all the electrolytes revealed extremely low silver dissolution, clarifying the absence of antibacterial effect of the films, which may indicate that not only the electrolyte components affect the silver release but also the matrix-Ag couple does not facilitate the silver ionization.

4. Conclusions

ZrCN–Ag coatings deposited by magnetron sputtering onto SS316L were tested as antibacterial materials, including the influence of the medium on the silver ion release due to its importance on the antimicrobial activity. The results evidenced a lack of antibacterial activity of the films, mainly explained due to the low silver release of the material in contact with the electrolytes. Although the silver ionization is highly

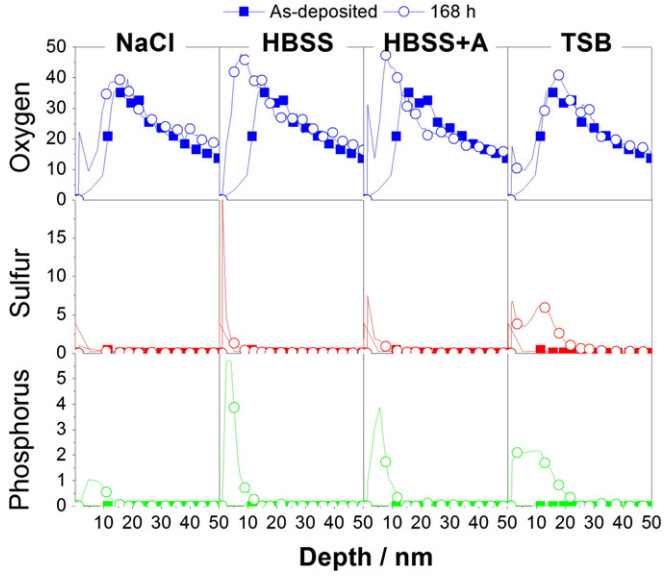

Fig. 7. Oxygen, sulfur and phosphorus depth profile of ZrCN–Ag for as-deposited (▪) samples and after 168 h (o) of immersion in NaCl, Hanks' balanced salt solution (HBSS), HBSS with 10 g of albumin per liter (HBSS + A), and tryptic soy broth (TBS). The lines represent the experimental results, while the symbols are used to differentiate the elements.

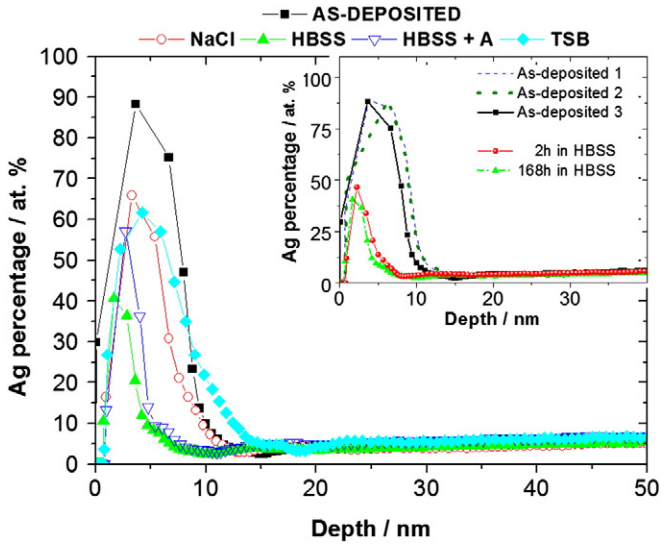

Fig. 9. Silver depth profile of ZrCN–Ag for as-deposited samples and after 168 h of immersion in NaCl, Hanks' balanced salt solution (HBSS), HBSS with 10 g of albumin per liter (HBSS + A), and tryptic soy broth (TBS). Inset: Silver depth profile for 3 different ZrCN–Ag as-deposited samples. The lines represent the experimental results, while the symbols are used to differentiate the elements.

dependent on the fluid composition, all the electrolytes revealed extremely low silver dissolution, elucidating the absence of antibacterial effect of the films. The chemical composition of the films showed changes only on the first 15 nm, including silver content reduction and surface oxidation, which occur in the first hours in contact with the media without further modification as time evolves. Oxides, phosphates and proteins form protective layers, blocking the paths for electrolyte to penetrate further in the films and probably reducing the silver ion release. However, the sulfates in the electrolyte increase silver ionization.

Finally, in order to exploit the multifunctional properties of ZrCN–Ag, more specifically the antibacterial activity, silver ion release must occur, and thus, further studies are required to focus on the activation and control of the silver in electrolytes simulating the body fluids. Such activation may include, but not be limited to electrical, electrochemical or chemical activation.

Acknowledgment

This research is partially sponsored by the FEDER funds through the program COMPETE — Programa Operacional Factores de Competitividade and by the Portuguese national funds through FCT—Fundação para a Ciência e a Tecnologia, under the projects ANTIMICROBCOAT — PTDC/CTM/102853/2008 and in the framework of the Strategic Projects PEST-C/FIS/UI607/2011, PEST-C/EME/UI0285/2011 and SFRH/BD/80947/2011.

This work has also been supported by the Ministerio de Ciencia e Innovacion of Spain through the Consolider-Ingenio 2010 Programme (CSD2008-00023) and through project RyC2007-0026.

References

[1] A. Montali, Injury 37 (2006) S81–S86.
[2] A. Simchi, E. Tamjid, F. Pishbin, A.R. Boccaccini, Nanomed. Nanotechn. Biol. Med. 7 (2011) 22–39.
[3] A.P. Serro, C. Completo, R. Colaço, F. dos Santos, C.L. da Silva, J.M.S. Cabral, H. Araújo, E. Pires, B. Saramago, Surf. Coat. Technol. 203 (2009) 3701–3707.
[4] N. Manninen, R.E. Galindo, N. Benito, N. Figueiredo, A. Cavaleiro, C. Palacio, S. Carvalho, J. Phys. D. Appl. Phys. 44 (2011) 375501.
[5] C.H. Lai, Y.Y. Chang, H.L. Huang, H.Y. Kao, Thin Solid Films 520 (5) (2011) 1525–1531.
[6] M. Balaceanu, T. Petreus, V. Braic, C. Zoita, A. Vladescu, C. Cotrutz, M. Braic, Surf. Coat. Technol. 204 (2010) 2046–2050.
[7] M. Braic, V. Braic, M. Balaceanu, A. Vladescu, C. Zoita, I. Titorencu, V. Jinga, Surf. Coat. Technol. 206 (4) (2011) 604–609.
[8] J. Hsieh, C. Tseng, Y. Chang, S. Chang, W. Wu, Surf. Coat. Technol. 202 (2008) 5586–5589.
[9] P. Kelly, H. Li, P. Benson, K. Whitehead, J. Verran, R. Arnell, I. Iordanova, Surf. Coat. Technol. 205 (2010) 1606–1610.
[10] O. Baghriche, J. Kiwi, C. Pulgarin, R. Sanjinés, J. Photochem. Photobiol. A 229 (2012) 39–45.
[11] C. Mulligan, D. Gall, Surf. Coat. Technol. 200 (2005) 1495–1500.
[12] S. Calderon Velasco, V. Lopez, C.F. Almeida Alves, A. Cavaleiro, S. Carvalho, Corros. Sci. 80 (2014) 229–236.
[13] A. Betts, D. Dowling, M. McConnell, C. Pope, Mater. Des. 26 (2005) 217–222.
[14] A.M. El-Kady, A.F. Ali, R.A. Rizk, M.M. Ahmed, Ceram. Int. 38 (2011) 177–188.
[15] C.N. Lok, C.M. Ho, R. Chen, Q.Y. He, W.Y. Yu, H. Sun, P.K.H. Tam, J.F. Chiu, C.M. Che, J. Biol. Inorg. Chem. 12 (2007) 527–534.
[16] H. Cao, X. Liu, F. Meng, P.K. Chu, Biomaterials 32 (2011) 693–705.
[17] D. Dowling, A. Betts, C. Pope, M. McConnell, R. Eloy, M. Arnaud, Surf. Coat. Technol. 163 (2003) 637–640.
[18] I. Sondi, B. Salopek-Sondi, J. Colloid Interface Sci. 275 (2004) 177–182.
[19] W.K. Jung, H.C. Koo, K.W. Kim, S. Shin, S.H. Kim, Y.H. Park, Appl. Environ. Microbiol. 74 (2008) 2171–2178.
[20] N.A. Monteiro-Riviere, M.E. Samberg, S.J. Oldenburg, J.E. Riviere, Toxicol. Lett. 220 (2013) 286–293.
[21] A. Ravindran, A. Singh, A.M. Raichur, N. Chandrasekaran, A. Mukherjee, Colloids Surf., B 76 (2010) 32–37.
[22] D.P. Gnanadhas, M.B. Thomas, R. Thomas, A.M. Raichur, D. Chakravortty, Antimicrob. Agents Chemother. 57 (2013) 4945–4955.
[23] C. Isabel, H. Mariana, O. João Carlos, A. Cristiana Filipa Almeida, P. Ana Paula, C. Sandra, Sci. Technol. Adv. Mater. 14 (2013) 035009.
[24] S. Calderon V, R. Escobar Galindo, N. Benito, C. Palacio, A. Cavaleiro, S. Carvalho, J. Phys. D. Appl. Phys. 46 (2013) 325303.
[25] R. Escobar Galindo, N.K. Manninen, C. Palacio, S. Carvalho, Anal. Bioanal. Chem. 405 (2013) 6259–6269.
[26] V.S.K. Chakravadhanula, Y.K. Mishra, V.G. Kotnur, D.K. Avasthi, T. Strunskus, V. Zaporotchenko, D. Fink, L. Kienle, F. Faupel, Beilstein J. Nanotechnol. 5 (2014) 1419–1431.
[27] N.K. Manninen, R.E. Galindo, S. Carvalho, A. Cavaleiro, Silver surface segregation in Ag–DLC nanocomposite coatings, Surf. Coat. Technol. 267 (2015) 90–97.
[28] D.J. Wickens, G. West, P.J. Kelly, J. Verran, S. Lynch, K.A. Whitehead, Int. J. Artif. Organs 35 (2012) 817–825.
[29] Z. Kertzman, J. Marchal, M. Suarez, M.H. Staia, P. Filip, P. Kohli, S.M. Aouadi, J. Biomed. Mater. Res. A 84A (2008) 1061–1067.
[30] C. Valero Vidal, A. Igual Muñoz, Electrochim. Acta 55 (2010) 8445–8452.
[31] K. Bayer, Influence of Capping Agents on Silver Nanoparticle (Ag–NP) Toxicity to Nitrifying Bacteria, San Diego State University, San Diego, 2012.